

## Shooting for Selective Druglike G-Quadruplex Binders: Evidence for Telomeric DNA Damage and Tumor Cell Death

Sandro Cosconati,<sup>†,⊥</sup> Angela Rizzo,<sup>‡,⊥</sup> Roberta Trotta,<sup>§</sup> Bruno Pagano,<sup>§</sup> Sara Iachettini,<sup>‡</sup> Stefano De Tito,<sup>§</sup> Iliara Lauri,<sup>§</sup> Iolanda Fotticchia,<sup>||</sup> Mariateresa Giustiniano,<sup>§</sup> Luciana Marinelli,<sup>§</sup> Concetta Giancola,<sup>||</sup> Ettore Novellino,<sup>§</sup> Annamaria Biroccio,<sup>\*,‡</sup> and Antonio Randazzo<sup>\*,§</sup>

<sup>†</sup>Dipartimento di Scienze Ambientali, Seconda Università di Napoli, 81100 Caserta, Italy

<sup>‡</sup>Experimental Chemotherapy Laboratory, Regina Elena National Cancer Institute, 00158 Rome, Italy

<sup>§</sup>Dipartimento di Chimica Farmaceutica e Tossicologica, Università di Napoli "Federico II", 80131 Napoli, Italy

<sup>||</sup>Dipartimento di Scienze Chimiche, Università di Napoli "Federico II", 80126, Naples, Italy

### **S** Supporting Information

**ABSTRACT:** Targeting of DNA secondary structures, such as G-quadruplexes, is now considered an appealing opportunity for drug intervention in anticancer therapy. So far, efforts made in the discovery of chemotypes able to target G-quadruplexes mainly succeeded in the identification of a number of polyaromatic compounds featuring end-stacking binding properties. Against this general trend, we were persuaded that the G-quadruplex grooves can recognize molecular entities with better drug-like and selectivity properties. From this idea, a set of small molecules was identified and the structural features responsible for G-quadruplex recognition were delineated. These compounds were demonstrated to have enhanced affinity and selectivity for the G-quadruplex over the duplex structure. Their ability to induce selective DNA damage at telomeric level and to induction of apoptosis and senescence on tumor cells is herein experimentally proven.



### **■ INTRODUCTION**

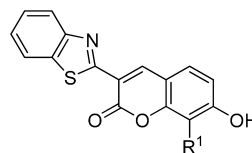
Telomeres are critical chromosomal elements which guarantee proper replication and protection of chromosome ends.<sup>1</sup> They are made up of 2–20 kb of double-stranded TTAGGG repeats and feature a 3' single-stranded overhang of 50–500 nucleotides. Parallel to normal cells proliferation, telomeres get gradually shorter triggering irreversible growth arrest (cellular senescence).<sup>2</sup> A telomere maintenance mechanism is provided by the six-membered protein complex called shelterin and by telomerase. The latter adds copies of the repeated motif to the end of the single-stranded overhang. This enzyme is transcriptionally repressed in most differentiated human somatic cells<sup>3</sup> while being overexpressed in about 85% of cancer cells.<sup>4</sup> In the remaining 15% of human tumors, telomere lengthening is obtained by a different mechanism known as alternative lengthening of telomere (ALT).<sup>5</sup> In both cases, telomeres are maintained to a stable length with consequent senescence circumvention and cellular immortalization.<sup>6</sup> In this scenario, it is now widely accepted that telomere maintenance and protection play a central role in tumorigenesis. Thus, agents that are able, at any level, to influence telomere homeostasis are considered now an appealing opportunity for drug intervention in anticancer therapy. The 3' single-stranded overhang of the telomeric DNA in eukaryotic cells can adopt the peculiar G-quadruplex fold.<sup>7</sup> The stabilization of this fold through the interaction with different ligands alters the G-rich overhang structure and causes its degradation through a DNA-

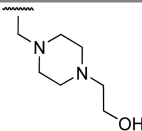
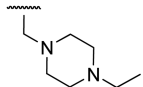
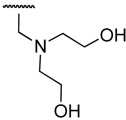
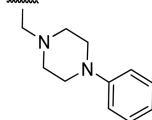
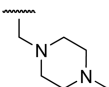
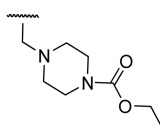
damage repair pathway and release of one of shelterin proteins (i.e., POT1) from telomeres.<sup>8</sup> These events lead to a fast induction of tumor cell senescence and apoptosis. For some of these compounds the *in vivo* anticancer activity has been reported (BRACO-19, RHSP4, and telomestatin).<sup>9–11</sup> Unfortunately, none of these molecules have progressed beyond the experimental stage into clinical trial, mainly because of insufficient druglike properties. Recently, our pursuit of new G-quadruplex ligands succeeded in the discovery of six leadlike chemotypes that were proven to effectively interact with the [d(TGGGGT)]<sub>4</sub> G-quadruplex structure.<sup>12</sup> Among them, compound **1a** (Table 1) appeared to be the most promising hit. So far, ligands that selectively recognize G-quadruplex grooves are few,<sup>13</sup> even though quadruplex groove recognition is likely to provide much more quadruplex-selective ligands. Interestingly, **1a** was proven to span the entire quadruplex grooves and was demonstrated to interact more tightly than distamycin A (Dst),<sup>14</sup> which was described as the most affine G-quadruplex groove binder.<sup>15</sup> More general considerations need to be done on the druglike properties of the **1a** coumarin core. This is a naturally occurring structure (mainly in plants) that is present in a plethora of compounds endowed with different biological activities (anti-HIV, CNS-active, anticoagulant, anti-inflammatory, antitumor).<sup>16</sup> Because of the

Received: July 12, 2012

Published: October 11, 2012

Table 1. Structures of the Selected Coumarin Derivatives



Cpd	R <sup>1</sup>	Cpd	R <sup>1</sup>
<b>1a</b>		<b>1d</b>	
<b>1b</b>		<b>1e</b>	
<b>1c</b>		<b>1f</b>	

number of documented biological activities and its amenability to combinatorial chemistry, the coumarin scaffold represents a well-known example of privileged structure.<sup>16</sup>

In the present study, the promising derivative **1a** was used as a seed for searching similar entities in several commercially available databases, and NMR experiments allowed identification of a small focused library of structural analogues with G-quadruplex binding properties. By a back and forth approach, the structural features responsible for G-quadruplex groove recognition were delineated, while isothermal titration calorimetry (ITC) measurements allowed for the identification of chemotypes featuring a tighter binding than Dst. Different from Dst, the best binders were also proved to be G-quadruplex selective over duplex. These results propelled the biological characterization of the new ligands, demonstrating their ability to induce selective DNA damage at telomeric level and induction of apoptosis and senescence on tumor cells.

## RESULTS AND DISCUSSION

**Compound Selection and G-Quadruplex NMR Binding Assays.** Given the relative synthetic accessibility of coumarin compounds, we first decided to search in commercial molecular databases if analogues of compound **1a** were available. This approach has the advantage of rapidly providing a library of structural analogues of the lead compound and also being highly economically efficient. Therefore, the simplistic pairwise Tanimoto similarity score was computed between **1a** and the compounds present in the full ZINC database collection of purchasable compounds (~7 million compounds) using a 70% similarity threshold. This resulted in 272 compounds that were visually analyzed revealing that, as expected, coumarin derivatives were selected (Table 1) as well as several analogues featuring the regioisomeric chromone scaffold (Table 2).

With the aim of exploring the influence of the pendant amine moiety on the quadruplex binding, five of the available coumarin derivatives derived from the filtered database were

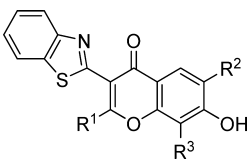
first purchased (**1b–f**). These were all tested for their ability to interact with the DNA quadruplex through nuclear magnetic resonance (NMR) spectroscopy, which is a valuable tool for studying molecular interactions in solution.<sup>17</sup> A number of DNA quadruplex folding topologies are known, and the kind of folding is strongly affected by the sequence, buffer, and molecular crowding conditions. This is particularly true for the human telomeric sequence.<sup>7</sup> In fact, several structures have been reported having different strand orientations and loop distributions. Unfortunately, the topology of the quadruplex structure adopted by the human telomeric sequence in vivo is unknown, so in analogy to what was done in our previous investigations,<sup>12,15</sup> we have decided to use the highly symmetric tetramolecular quadruplex [d(TGGGGT)]<sub>4</sub>. In particular, we employed the chemical shift perturbation method<sup>18</sup> to detect interaction between a molecular candidate and the G-quadruplex structure. The signals that can be most easily monitored are the imino and aromatic protons of all bases and the methyl protons of thymines, as they all are in the less crowded region of the NMR spectrum of [d(TGGGGT)]<sub>4</sub>.

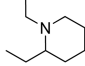
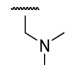
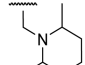
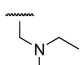
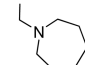
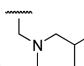
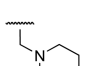
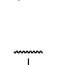
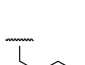

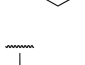
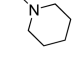

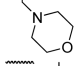
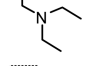
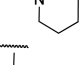
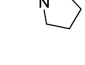
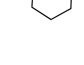
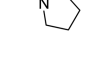
Since we were mainly interested in potential groove binder analogues, in our inspection we considered quadruplex ligands all compounds providing a shift of the G3 and G4 signals of at least 0.05 ppm. Following this criterion, among the five tested coumarins, compounds **1b–d** demonstrated appreciable G-quadruplex binding while **1e** and **1f** displayed no DNA interaction. This indicates that the presence a H-bond donor (**1b**) and/or a positively charged group at a distal position (**1c–d**) with respect to the coumarin scaffold is critical for DNA binding.

More structural variability was present when considering the regioisomeric chromone derivatives (**2a–k**, Table 2). This moiety is also regarded as a privileged structure, being present in different biologically active compounds and prone to combinatorial synthesis.<sup>19</sup> In this case, we first tested the G-quadruplex binding properties of **2a** through NMR titration. This experiment did not indicate appreciable shift of any signal of [d(TGGGGT)]<sub>4</sub>, suggesting that the chromone scaffold is unable to provide efficient binding for the quadruplex. On the other hand, the positively charged group in position 8 (R<sup>3</sup> substituent) should provide this moiety with a critical interaction point with the quadruplex (most probably, with the phosphate backbone atoms), as confirmed by the presence of detectable interactions of compounds **2b** and **2c** with the target. Furthermore, bulky tertiary amines are not tolerated (**2d**), while cyclic amines (**2e–k**) are able to cause substantial shift of the G3, G4, G5, and T6 signals. In order to probe the influence of a substituent in position 2 on the chromone scaffold (R<sup>1</sup> in Table 2), **2l–p**, featuring H-bond donor groups, were also tested. Interestingly, while **2l–o** still provide appreciable quadruplex binding, **2p** does not interact with the DNA, suggesting that bulkier amines are detrimental for the binding regardless of the presence of a H-bond donor in position 2. Indeed, the latter position seems to directly influence the G-quadruplex recognition, considering that the simple substitution with a methyl group (**2s–t**) abolishes the ligand binding as demonstrated by NMR experiments. The same holds true for position 6 (R<sup>2</sup>) of the chromone ring that when substituted with an ethyl chain results in compounds **2q–r**, which are incapable of [d(TGGGGT)]<sub>4</sub> binding.

**Isothermal Titration Calorimetry (ITC) Experiments.** For compounds demonstrating appreciable interaction with the DNA G-quadruplex (**1a,b**, **2b,c**, **2e–o**) displacement iso-

Table 2. Structures of the Selected Chromone Derivatives



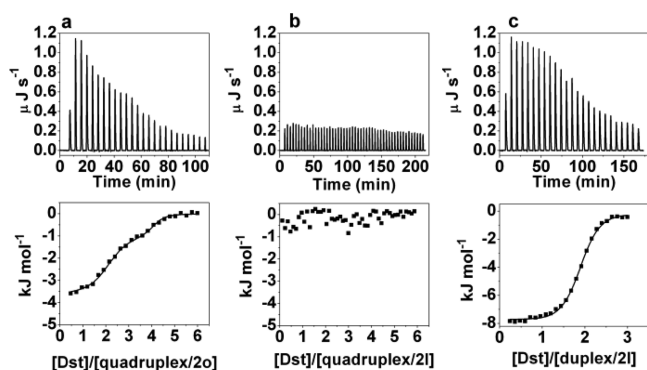
Cpd	R <sup>1</sup>	R <sup>2</sup>	R <sup>3</sup>	Cpd	R <sup>1</sup>	R <sup>2</sup>	R <sup>3</sup>
2a	-H	-H	-H	2k	-H	-H	
2b	-H	-H		2l	-NH <sub>2</sub>	-H	
2c	-H	-H		2m	-NH <sub>2</sub>	-H	
2d	-H	-H		2n	-NH <sub>2</sub>	-H	
2e	-H	-H		2o	-NH <sub>2</sub>	-H	
2f	-H	-H		2p	-NH <sub>2</sub>	-H	
2g	-H	-H		2q	-H	-CH <sub>2</sub> CH <sub>3</sub>	
2h	-H	-H		2r	-H	-CH <sub>2</sub> CH <sub>3</sub>	
2i	-H	-H		2s	-CH <sub>3</sub>	-H	
2j	-H	-H		2t	-CH <sub>3</sub>	-H	

thermal titration calorimetry (ITC) experiments<sup>20</sup> were performed to investigate their quadruplex binding affinity. Since it is well-known that multiple conformations of the human telomeric sequences may coexist in solution and that such polymorphism could invalidate the data obtained by ITC measurements, we have decided to use, in analogy to NMR, the [d(TGGGGT)]<sub>4</sub> quadruplex.

Unfortunately, efforts to obtain direct thermodynamic information from canonical ITC experiments failed because of solubility issues regarding the ligands at the rather high concentrations required for such measurements.<sup>21</sup> Displacement experiments were then effectively carried out by analyzing the binding of Dst to the G-quadruplex previously saturated with each ligand (see Experimental Section). Although the displacement ITC experiments do not allow direct measurement of the thermodynamic parameters involved in the binding processes, this strategy represents a valid approach for evaluating the efficiency of a G-quadruplex (or duplex) binder

compared to Dst. Indeed, when the DNA–ligand complex is formed, the ligand will inhibit the binding of Dst if its affinity for the G-quadruplex is higher than the latter; conversely, it will be displaced by a stronger binder.

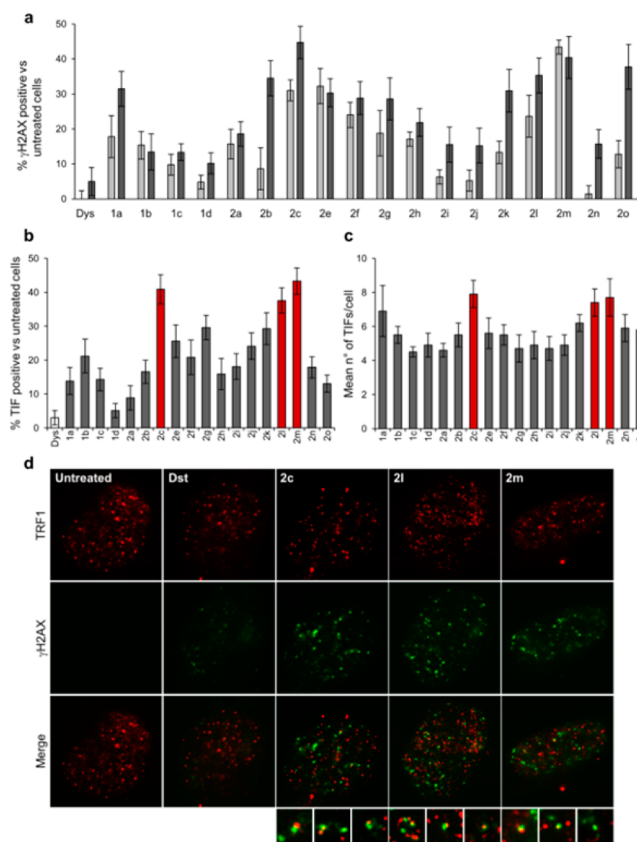
Figure 1a and Figure 1b show two representative ITC displacement experiments carried out by titrating with Dst the [d(TGGGGT)]<sub>4</sub> saturated with compounds **2o** and **2l**, respectively. The results obtained in the two experiments clearly show two different phenomena. In the first case, the ITC profile for the titration of ligand-saturated G-quadruplex is essentially identical to the one obtained for the binding of Dst to the G-quadruplex alone,<sup>14</sup> thus indicating that the presence of **2o** does not affect significantly the interaction. On the contrary, the titration of [d(TGGGGT)]<sub>4</sub>/**2l** mixture with Dst (Figure 1b) gives completely different results. In this case, ITC data show constant heat release at each injection of Dst, only due to ligand dilution, proving that it is no longer able to interact with the G-quadruplex. Overall, ITC experiments



**Figure 1.** Raw ITC data (top panels) and integrated heat (bottom panels) for titration of  $[d(\text{TGGGGT})]_4/2\text{o}$  (a),  $[d(\text{TGGGGT})]_4/2\text{l}$  (b), and  $d(\text{CGCGAATTCGCG})_2/2\text{l}$  (c) mixtures with Dst at 25 °C. The integrated heat for the titrations (squares) was obtained by integrating the raw data and subtracting the heat of the ligand dilution. The lines represent nonlinear least-squares fit of the data to the appropriate binding model.

showed that 4 out of 15 compounds (**1a**, **2c**, **2l**, and **2m**) have the ability to bind the G-quadruplex more tightly than Dst, inhibiting its interaction. To evaluate a possible selectivity of the best ligands for G-quadruplex over duplex, we performed identical ITC displacement experiments by titrating  $d(\text{CGCGAATTCGCG})_2$  duplex/ligand mixtures with Dst. This self-complementary DNA dodecamer was chosen because it contains the central AATT core, considered being one of the specific binding sites for Dst.<sup>22</sup> Figure 1c shows an example of raw ITC data and binding isotherm for the titration of  $d(\text{CGCGAATTCGCG})_2/2\text{l}$  mixture with Dst. As shown, at each injection of Dst solution, less and less heat release was measured until constant values were obtained, implying a saturable process. The binding isotherm shows a typical sigmoidal binding curve and clearly suggests that the presence of the compound in the mixture has no effect on the interaction of Dst with the duplex. Similar results were obtained for **2c** and **2m** (see Supporting Information), suggesting G-quadruplex selectivity of these three compounds. On the other hand, **1a** was shown to affect Dst-duplex interaction, thus suggesting a poor selectivity.

**The Newly Identified G-Quadruplex Ligands Induce DNA Damage and Cell-Cycle Arrest.** These encouraging results propelled the full biological characterization of the new ligands for investigating the ability of the new ligands to cause telomere uncapping (Figure 2). To this aim, a two-step analysis was performed to establish, in the first one, if the compounds were able to induce DNA damage and, in the second one, if the DNA damage was localized to the telomeres. By using human transformed BJ fibroblasts (BJ-EHLT), we found that, different from Dst, all the ligands were able to induce DNA damage (at least at the higher drug dose, Figure 2a) and deconvolution microscopy analysis showed that some of the damaged foci colocalized with TRF1, a good marker for interphase telomeres<sup>23</sup> forming the so-called TIF (telomere dysfunction induced foci)<sup>24</sup> (Figure 2d). Of note, quantitative analysis identified compounds **2c**, **2l**, and **2m** as the most potent in inducing telomere damage: the percentage of cells with more than four  $\gamma\text{H2AX}/\text{TRF1}$  colocalizations reached about 50% (Figure 2b), with a mean of about eight TIF per nucleus (Figure 2c). Such a biological evaluation also confirmed that the sole chromone structure (**2a**) was not proved to cause

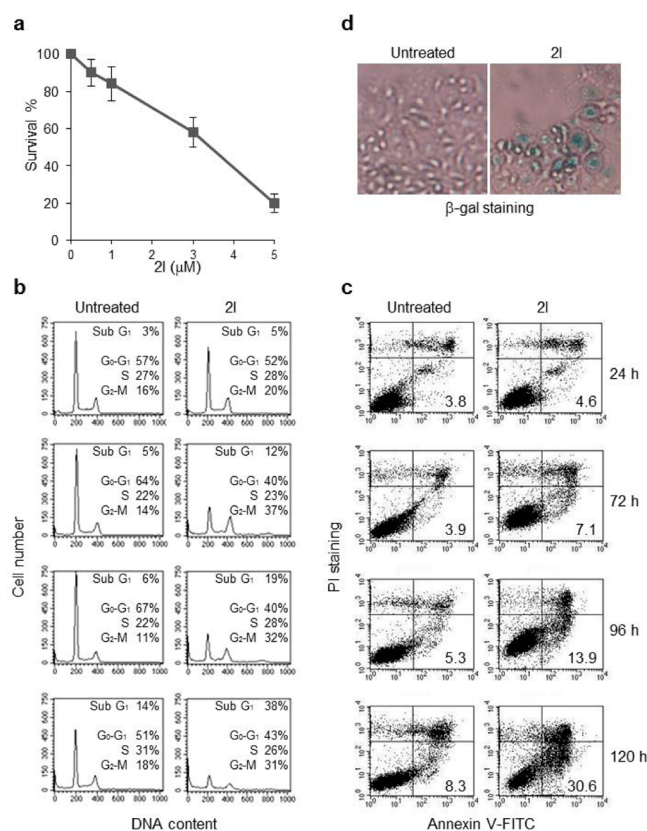


**Figure 2.** DNA damage activation at telomeres. BJ-EHLT fibroblasts were treated for 24 h with Dst and the indicated ligands at doses 0.1 (light-gray bars) and 0.5  $\mu\text{M}$  (dark-gray bars). Cells were processed for immunofluorescence (IF) using antibodies against  $\gamma\text{H2AX}$  and TRF1 to mark DNA damage and telomeres, respectively. Percentages of  $\gamma\text{H2AX}$ -positive (a) and TIF-positive (b) treated vs untreated cells are reported in the histograms. (c) Mean number of TIF/cell in the indicated samples. Cells with four or more  $\gamma\text{H2AX}/\text{TRF1}$  foci were scored as TIF positive. The red bars highlight the most effective ligands. Error bars indicate the standard deviation. (d) Representative images of IF of untreated and Dst-, **2c**-, **2l**-, and **2m**-treated BJ-EHLT cells. Enlarged views of TIFs are reported below the merged images. The images were acquired with a Leica deconvolution microscope (magnification 100 $\times$ ).

substantial DNA damage. Interestingly, the whole data are in perfect consonance with ITC experiments that indicated that **2c**, **2l**, and **2m** are strong, selective G-quadruplex binders. A further correlation can also be done for compound **1a** that, by promiscuously binding the DNA (see ITC data), is able to induce high levels of DNA damage but few TIFs.

The above results raised the interesting possibility that telomere damages induced by the ligands in transformed fibroblasts may rapidly and efficiently promote growth inhibition in tumor cells. Treatment of HeLa cells with one of the most promising selected ligands (**2l**) triggered a dose-dependent inhibition of cell survival (Figure 3a) associated with an early accumulation of cells in the  $\text{G}_2/\text{M}$  phase of the cell cycle, and at 96 h of treatment a fraction of cell population resided in the sub- $\text{G}_1$  compartment, indicative of apoptosis (Figure 2b).

Apoptosis induction triggered by **2l** has been confirmed by annexin staining (Figure 3c; at 96 h of treatment about 30% of cells are annexin V-positive/PI negative), and it was also accompanied by the induction of a senescence phenotype: large



**Figure 3.** Biological effects of **2l** ligand. (a) Survival curve of the HeLa cells exposed to different doses of **2l** ranging from 0.5 to 5 μM. (b) Cell cycle analysis and (c) apoptosis evaluation of HeLa cells processed at the indicated times after exposure with 3.5 μM **2l**. (c) Biparametric dot plots showing PI vs annexin V staining in the indicated samples. (d) SA-β-gal staining of HeLa cells untreated and treated with 5 μM **2l** for 5 days.

cell size, vacuolated cytoplasm, and β-galactosidase activity (Figure 3d).

**The Newly Identified G-Quadruplex Ligands Feature Enhanced Druglikeness.** In our inspection, the most interesting ligands (**1a**, **2c**, **2l**, and **2m**) were also compared for their predicted absorption, distribution, metabolism, and excretion (ADME) properties with respect to other compounds previously described as G-quadruplex binders (Supporting Information, Table S3). These calculations were performed employing the QikProp software (QikProp, version 3.4 (2011); Schrödinger, LLC, New York, NY). In addition to predicting molecular properties, QikProp provides ranges for comparing each compound's property with those of 95% of known drugs (these ranges are provided in Supporting Information, Table S4). This software was also used because it allows for flagging reactive functional groups that may cause false positives in biological assays. Results of QikProp calculations are reported in Supporting Information, Tables S5–S7. According to these calculations, only 7 out of 32 inspected compounds display no violations of the ranges recommended for each descriptor or property. Strikingly, compounds **1a**, **2c**, **2l**, and **2m** are among these most promising ligands.

## CONCLUSIONS

Targeting of DNA secondary structures such as G-quadruplexes is now considered an appealing opportunity for drug

intervention in anticancer therapy.<sup>25</sup> So far, efforts made in the discovery of chemotypes able to target G-quadruplexes mainly succeeded in the identification of a number of polyaromatic compounds featuring end-stacking binding properties. Unfortunately, the poor druglike properties of these compounds turned out to be a main limitation during the in vivo verification of their antitumor properties. Herein, with the aim of discovering G-quadruplex groove binders with enhanced druglike properties, a lead optimization campaign was undertaken starting from a promising virtual screening hit. Thus, the physicochemical characterization (NMR and ITC) of the binding of a set of closely related analogues allowed identification of novel ligands of the [d(TGGGGT)]<sub>4</sub> quadruplex. Interestingly, their biological characterization demonstrated the ability to induce selective DNA damage at telomeric level and induction of apoptosis and senescence on tumor cells. These results substantiate our choice of using the [d(TGGGGT)]<sub>4</sub> structure as a working model to design new molecular entities endowed with G-quadruplex binding properties. Furthermore, for the first time, we demonstrate that selective G-quadruplex binding and telomeric DNA damage can be elicited by more druglike chemotypes. These findings pave the way for the design of new potential drugs and shed new insights into the emerging field of DNA quadruplex.

## EXPERIMENTAL SECTION

**Oligonucleotide Synthesis.** The oligonucleotide d(TGGGGT) was synthesized using standard protocol.<sup>26</sup> The oligomer was detached from the support and deprotected by treatment with concentrated aqueous ammonia at 55 °C for 12 h. The combined filtrates and washings were concentrated under reduced pressure, redissolved in H<sub>2</sub>O, analyzed, and purified by high-performance liquid chromatography (HPLC) on a Nucleogel SAX column (Macherey-Nagel, 1000-8/46), using buffer A consisting of 20 mM KH<sub>2</sub>PO<sub>4</sub>/K<sub>2</sub>HPO<sub>4</sub> aqueous solution (pH 7.0), containing 20% (v/v) CH<sub>3</sub>CN, buffer B consisting of 1 M KCl, 20 mM KH<sub>2</sub>PO<sub>4</sub>/K<sub>2</sub>HPO<sub>4</sub> aqueous solution (pH 7.0), containing 20% (v/v) CH<sub>3</sub>CN, a linear gradient from 0% to 100% B for 30 min, and flow rate 1 mL/min. The fractions of the oligomer were collected and successively desalted by Sep-pak cartridges (C-18). The isolated oligomer proved to be >99% pure by NMR.

**Selected Compounds.** The selected compounds were purchased from the supplier as indicated in Table S1 (see Supporting Information). The purity of compounds **1a–f** and **2a–t** was assessed using reversed-phase high-performance liquid chromatography (HPLC), using a Shimadzu C18, 5 μm (150 mm × 4.6 mm) column. The elution was performed with a 1.0 mL/min flow rate using a linear gradient from 0% to 100% methanol in water over 30 min. The detection was performed at 210 nm. The purity was also analyzed with high-performance liquid chromatography–mass spectrometry (HPLC–MS) performed on an Agilent 1200 series system (Agilent Technologies, Santa Clara, CA, USA) equipped with an Agilent 6110 series LC/MS quadrupole instrument, using a Phenomenex Luna C18, 5 μm (150 mm × 4.6 mm) column. The elution was performed with a 1.0 mL/min flow rate using a linear gradient from 0% to 90% acetonitrile in water over 20 min. Detection was performed at 210 nm. The relative purity of compounds **1a**, **1c–e**, **2a–d**, **2f**, **2h**, **2i**, **2l–n**, and **2p–r** was higher than 98.0%. Purity of compounds **1b**, **1f**, **2e**, **2g**, **2j**, **2k**, **2o**, **2s**, and **2t** ranged between 95% and 98%.

**Nuclear Magnetic Resonance Experiments.** The quadruplex NMR samples were prepared at 0.1 mM (0.4 mM single strand concentration) in 0.2 mL (H<sub>2</sub>O/D<sub>2</sub>O, 9:1) of buffer solution having 10 mM KH<sub>2</sub>PO<sub>4</sub>, 70 mM KCl, 0.2 mM EDTA, pH 7.0. NMR spectra were recorded with Varian Unity INOVA 700 MHz spectrometer. <sup>1</sup>H chemical shifts were referenced to external sodium 2,2-dimethyl-2-silapentane-5-sulfonate (DSS). 1D proton spectra of the sample in H<sub>2</sub>O were recorded using pulsed-field gradient DPGFSE<sup>27,28</sup> for H<sub>2</sub>O

suppression. The NMR data were processed on an iMAC running iNMR software ([www.inmr.net](http://www.inmr.net)).

**Chemical Shift Perturbation Experiments.** The quadruplex  $[d(\text{TGGGGT})]_4$  has been titrated with each of the selected compounds. The samples **1e–f**, **2a**, **2d**, **2p–t** were not able to cause any significant shift of the DNA signals. On the other hand, the compounds **1b–d**, **2b**, **2c**, **2e–k**, **2l–o** turned out to be able to bind the quadruplex. Particularly, for all the titrations of **1b–d**, **2b**, **2c**, **2e–k**, **2l–o**, the four DNA strands turned out to be magnetically equivalent throughout the titration, and no splitting of resonances was observed at any stage. In order to preliminarily evaluate the binding site of each analogue, a comparison of resonances of some protons of the uncomplexed DNA and the complexed one has been done. In particular, we report the  $\Delta\delta$  values (chemical shifts of the complex minus free DNA) of aromatic, methyl, and imino protons (Supporting Information, Table S2). Generally, the signals of the protons of the T1 residue shifted the least, whereas the ones of residue T6 shifted more. In any case, a general shift of the aromatic and imino signals was also observed for the G2, G3, G4, and G5.

**Isothermal Titration Calorimetry.** The  $d(\text{TGGGGT})$  and  $d(\text{CGCGAATTCGCG})$  oligonucleotide sequences were prepared by dissolving the lyophilized compound in 10 mM phosphate buffer with 70 mM KCl, 0.2 mM EDTA, pH 7. The solutions were annealed by heating at 90 °C for 5 min and slowly cooling to room temperature and then equilibrated at 4 °C for 24 h. The concentration of oligonucleotides was determined by UV adsorption measurements at 90 °C using molar extinction coefficient values  $\epsilon_{(260\text{ nm})}$  of 57 800 and 110 700  $\text{M}^{-1}\text{ cm}^{-1}$  for  $d(\text{TGGGGT})$  and  $d(\text{CGCGAATTCGCG})$ , respectively. The molar extinction coefficients were calculated by the nearest neighbor model.<sup>29</sup> Stock solutions of the investigated compounds were prepared by solubilizing weighted amounts in DMSO to a final concentration of 8 mM. The mixtures of the DNA molecules and the compounds were prepared by diluting the ligand stock solution into the DNA solution to get a final ligand/DNA molar ratio of 4:1 and a final DMSO concentration of 7%. Dst was solubilized in the same buffer used for the mixtures. ITC experiments were performed at 298 K using a CSC 5300 Nano-ITC microcalorimeter from Calorimetry Science Inc. (Lindon, UT) with a cell volume of 1 mL. The titrations were carried out in 10 mM phosphate buffer, 70 mM KCl, 0.2 mM EDTA, 7% DMSO, pH 7. In each experiment, volumes of 5–10  $\mu\text{L}$  of Dst solution (360–720  $\mu\text{M}$ ) were added into a 30  $\mu\text{M}$  solution of DNA or DNA/ligand mixture, using a computer-controlled 250  $\mu\text{L}$  microsyringe, with a spacing of 200–400 s between each injection. Each titration was corrected by subtracting the heat of Dst dilution. Where possible, integrated heat data obtained for the titrations were fitted by employing a nonlinear least-squares minimization algorithm to a theoretical titration curve, using the Bindwork software from Calorimetry Science Inc.

**Cells and Culture Conditions.** Transformed human BJ fibroblasts expressing hTERT and SV40 early region (BJ-HELT) and human epithelial carcinoma cell line (HeLa) were obtained as previously reported<sup>8</sup> and grown in Dulbecco modified Eagle medium (D-MEM, Invitrogen Carlsbad, CA, U.S.) supplemented with 10% fetal calf serum, 2 mM L-glutamin, and antibiotics.

**Immunofluorescence.** Immunofluorescence was performed as previously reported.<sup>30</sup> Cells were fixed in 2% formaldehyde and permeabilized in 0.25% Triton-X100 in PBS for 5 min at room temperature. For immunolabeling experiments, cells were incubated with primary antibody, then washed in PBS and incubated with the secondary antibodies. The following primary antibodies were used: pAb anti-TRF1 (Abcam Ltd.; Cambridge, U.K.); mAb anti- $\gamma\text{H2AX}$  (Upstate; Lake Placid, NY). The following secondary antibodies were used: TRITC conjugated goat anti-rabbit, FITC conjugated goat anti-mouse (The Jackson Laboratory). Fluorescence signals were recorded by using a Leica DMIRE2 microscope equipped with a Leica DFC 350FX camera and elaborated by a Leica FW4000 deconvolution software (Leica, Solms, Germany).

**Clonogenic Assay.** HeLa cells were seeded in 60 mm Petri dishes (Nunc, MasciaBrunelli, Milan, Italy) at a density of  $5 \times 10^2$  cells per dish and 24 h later exposed to different doses (ranging from 0.5 to 5

mM) of **2m**. Cell colony-forming ability was determined as previously described.<sup>30</sup> All the experiments were repeated four times in triplicate.

**Flow Cytometric Analysis.** The cell cycle analysis was performed by flow cytometry. Cells were washed in PBS and fixed in 70% ethanol in PBS.  $1 \times 10^6$  cells were centrifuged and resuspended in a staining solution (50  $\mu\text{g}/\text{mL}$  PI, 75 kU/mL RNase A in PBS) for 30 min at room temperature in the dark and analyzed by flow cytometry using FACScalibur (Becton-Dickinson, San Jose, CA, U.S.). For each analysis 20 000 events were collected. Cell cycle distribution and percentage of apoptotic cells were analyzed using Cell Quest (BDIS) and ModFit LT (Verity Software House, Topsham, ME).

**Evaluation of Apoptosis.** Apoptosis was detected by flow cytometric analysis of annexin V staining. Annexin V-FITC vs PI assay (Vibrant apoptosis assay, V-13242, Molecular Probes, Eugene, OR, U.S.) was performed as previously described.<sup>31</sup> Briefly, adherent cells were harvested and suspended in the annexin-binding buffer ( $1 \times 10^6$  cells/mL). Thereafter, cells were incubated with annexin V-FITC and PI for 15 min at room temperature in the dark and immediately analyzed by flow cytometry. The data are presented as biparametric dot plots showing PI red fluorescence vs annexin V-FITC green fluorescence.

**Senescence Analysis.** Senescence-associated  $\beta$ -galactosidase (SA- $\beta$ -gal) staining on HeLa cells was performed as described by Dimri et al.<sup>32</sup> Briefly, after exposure with 3.5  $\mu\text{M}$  **2m** for 5 days to cell culture, the cells were fixed with 2% glutaraldehyde in PBS for 5 min at room temperature, washed in PBS, and incubated at 37 °C for 24 h in staining solution: 1 mg/mL 5-bromo-4-chloro-3-indolyl- $\beta$ -D-galactoside (X-gal), 5 mM potassium ferrocyanide, 5 mM potassium ferricyanide, 2 mM  $\text{MgCl}_2$  in PBS, pH 6.0. Then cells were analyzed using an optical microscope.

**Statistical Analysis.** The experiments have been repeated from three to five times, and the results obtained are presented as the mean  $\pm$  SD. Significant changes were assessed by using Student's *t* test for unpaired data, and  $P < 0.05$  was considered significant.

## ■ ASSOCIATED CONTENT

### 📄 Supporting Information

Vendor codes and suppliers for each tested compound; differences in chemical shifts ( $\Delta\delta$ ) of selected signals of DNA upon binding of derivatives **1b–d** and **2b,c,e–k,l–o**; additional isothermal titration calorimetry experiments; results of QikProp calculations. This material is available free of charge via the Internet at <http://pubs.acs.org>.

## ■ AUTHOR INFORMATION

### Corresponding Author

\*For A.B.: phone, +39-06-52662569; e-mail, [biroccio@ifo.it](mailto:biroccio@ifo.it). For A.R.: phone, +39-081-678514; e-mail, [antonio.randazzo@unina.it](mailto:antonio.randazzo@unina.it).

### Author Contributions

<sup>†</sup>These authors contributed equally.

### Notes

The authors declare no competing financial interest.

## ■ ACKNOWLEDGMENTS

Thanks are due to Carmen D'Angelo for flow cytometric analysis. This work was supported by the Italian Institute of Technology (IIT), Italian Association for Cancer Research (A.I.R.C. No. 11567 and No. 11947), and Italian MIUR (PRIN 2009). S.I. is recipient of fellowships from Italian Foundation for Cancer Research (FIRC).

## ■ ABBREVIATIONS USED

NMR, nuclear magnetic resonance; ITC, isothermal titration calorimetry; ALT, alternative lengthening of telomere; TIF, telomere dysfunction induced foci

## ■ REFERENCES

- (1) de Lange, T. Shelterin: the protein complex that shapes and safeguards human telomeres. *Genes Dev.* **2005**, *19*, 2100–2110.
- (2) Blackburn, E. H. Switching and signaling at the telomere. *Cell* **2001**, *106*, 661–673.
- (3) Lin, S. Y.; Elledge, S. J. Multiple tumor suppressor pathways negatively regulate telomerase. *Cell* **2003**, *113*, 881–889.
- (4) Kim, N. W.; Piatyszek, M. A.; Prowse, K. R.; Harley, C. B.; West, M. D.; Ho, P. L.; Coviello, G. M.; Wright, W. E.; Weinrich, S. L.; Shay, J. W. Specific association of human telomerase activity with immortal cells and cancer. *Science* **1994**, *266*, 2011–2015.
- (5) Cesare, A. J.; Reddel, R. R. Telomere uncapping and alternative lengthening of telomeres. *Mech. Ageing Dev.* **2008**, *129*, 99–108.
- (6) Bodnar, A. G.; Ouellette, M.; Frolkis, M.; Holt, S. E.; Chiu, C. P.; Morin, G. B.; Harley, C. B.; Shay, J. W.; Lichtsteiner, S.; Wright, W. E. Extension of life-span by introduction of telomerase into normal human cells. *Science* **1998**, *279*, 349–352.
- (7) (a) Chaires, J. B. Human telomeric G-quadruplex: thermodynamic and kinetic studies of telomeric quadruplex stability. *FEBS J.* **2010**, *277*, 1098–1106. (b) Phan, A. T. Human telomeric G-quadruplex: structures of DNA and RNA sequences. *FEBS J.* **2010**, *277*, 1107–1117.
- (8) (a) Gomez, D.; O'Donohue, M. F.; Wenner, T.; Douarre, C.; Macadré, J.; Koebel, P.; Giraud-Panis, M. J.; Kaplan, H.; Kolkes, A.; Shin-ya, K.; Riou, J. F. The G-quadruplex ligand telomestatin inhibits POT1 binding to telomeric sequences in vitro and induces GFP-POT1 dissociation from telomeres in human cells. *Cancer Res.* **2006**, *66*, 6908–6912. (b) Pagano, B.; Giancola, C. Energetics of quadruplex-drug recognition in anticancer therapy. *Curr. Cancer Drug Targets* **2007**, *7*, 520–540. (c) Salvati, E.; Leonetti, C.; Rizzo, A.; Scarsella, M.; Mottolose, M.; Galati, R.; Sperduti, I.; Stevens, M. F.; D'Incalci, M.; Blasco, M.; Chiorino, G.; Bauwens, S.; Horard, B.; Gilson, E.; Stoppacciaro, A.; Zupi, G.; Biroccio, A. Telomere damage induced by the G-quadruplex ligand RHPS4 has an antitumor effect. *J. Clin. Invest.* **2007**, *117*, 3236–3247.
- (9) Burger, A. M.; Dai, F.; Schultes, C. M.; Reszka, A. P.; Moore, M. J.; Double, J. A.; Neidle, S. The G-quadruplex-interactive molecule BRACO-19 inhibits tumor growth, consistent with telomere targeting and interference with telomerase function. *Cancer Res.* **2005**, *65*, 1489–1496.
- (10) Phatak, P.; Cookson, J. C.; Dai, F.; Smith, V.; Gartenhaus, R. B.; Stevens, M. F.; Burger, A. M. Telomere uncapping by the G-quadruplex ligand RHPS4 inhibits clonogenic tumour cell growth in vitro and in vivo consistent with a cancer stem cell targeting mechanism. *Br. J. Cancer* **2007**, *96*, 1223–1233.
- (11) Tauchi, T.; Shin-ya, K.; Sashida, G.; Sumi, M.; Okabe, S.; Ohyashiki, J. H.; Ohyashiki, K. Telomerase inhibition with a novel G-quadruplex-interactive agent, telomestatin: in vitro and in vivo studies in acute leukemia. *Oncogene* **2006**, *25*, 5719–5725.
- (12) Cosconati, S.; Marinelli, L.; Trotta, R.; Virno, A.; Mayol, L.; Novellino, E.; Olson, A. J.; Randazzo, A. Tandem application of virtual screening and NMR experiments in the discovery of brand new DNA quadruplex groove binders. *J. Am. Chem. Soc.* **2009**, *131*, 16336–16337.
- (13) (a) Li, Q.; Xiang, J.; Li, X.; Chen, L.; Xu, X.; Tang, Y.; Zhou, Q.; Li, L.; Zhang, H.; Sun, H.; Guan, A.; Yang, Q.; Yang, S.; Xu, G. Stabilizing parallel G-quadruplex DNA by a new class of ligands: two non-planar alkaloids through interaction in lateral grooves. *Biochimie* **2009**, *91*, 811–829. (b) Ranjan, N.; Andreassen, K. F.; Kumar, S.; Hyde-Volpe, D.; Arya, D. P. Aminoglycoside binding to *Oxytricha nova* telomeric DNA. *Biochemistry* **2010**, *49*, 9891–9903. (c) Hamon, F.; Largy, E.; Guédin-Beaupaire, A.; Rouchon-Dagois, M.; Sidibe, A.; Monchaud, D.; Mergny, J. L.; Riou, J. F.; Nguyen, C. H.; Teulade-Fichou, M. P. An acyclic oligoheteroaryl that discriminates strongly between diverse G-quadruplex topologies. *Angew. Chem., Int. Ed.* **2011**, *50*, 8745–8749.
- (14) Trotta, R.; De Tito, S.; Lauri, I.; La Pietra, V.; Marinelli, L.; Cosconati, S.; Martino, L.; Conte, M. R.; Mayol, L.; Novellino, E.; Randazzo, A. A more detailed picture of the interactions between virtual screening-derived hits and the DNA G-quadruplex: NMR, molecular modelling and ITC studies. *Biochimie* **2011**, *93*, 1280–1287.
- (15) (a) Randazzo, A.; Galeone, A.; Mayol, L. <sup>1</sup>H-NMR study of the interaction of distamycin A and netropsin with the parallel stranded tetraplex [d(TGGGGT)]<sub>4</sub>. *Chem. Commun.* **2001**, *11*, 1030–1031. (b) Randazzo, A.; Galeone, A.; Esposito, V.; Varra, M.; Mayol, L. Interaction of distamycin A and netropsin with quadruplex and duplex structures: a comparative <sup>1</sup>H-NMR study. *Nucleosides, Nucleotides Nucleic Acids* **2002**, *21*, 535–545. (c) Martino, L.; Virno, A.; Pagano, B.; Virgilio, A.; Di Micco, S.; Galeone, A.; Giancola, C.; Bifulco, G.; Mayol, L.; Randazzo, A. Structural and thermodynamic studies of the interaction of distamycin A with the parallel quadruplex structure [d(TGGGGT)]<sub>4</sub>. *J. Am. Chem. Soc.* **2007**, *129*, 16048–16056. (d) Pagano, B.; Virno, A.; Mattia, C. A.; Mayol, L.; Randazzo, A.; Giancola, C. Targeting DNA quadruplexes with distamycin A and its derivatives: an ITC and NMR study. *Biochimie* **2008**, *90*, 1224–12232. (e) Cosconati, S.; Marinelli, L.; Trotta, R.; Virno, A.; De Tito, S.; Romagnoli, R.; Pagano, B.; Limongelli, V.; Giancola, C.; Baraldi, P. G.; Mayol, L.; Novellino, E.; Randazzo, A. Structural and conformational requisites in DNA quadruplex groove binding: another piece to the puzzle. *J. Am. Chem. Soc.* **2010**, *132*, 6425–6433.
- (16) Borges, F.; Roleira, F.; Milhazes, N.; Santana, L.; Uriarte, E. Simple coumarins and analogues in medicinal chemistry: occurrence, synthesis and biological activity. *Curr. Med. Chem.* **2005**, *12*, 887–916.
- (17) Petraccone, L.; Fotticchia, I.; Cummaro, A.; Pagano, B.; Ginnari-Satriani, L.; Haider, S.; Randazzo, A.; Novellino, E.; Neidle, S.; Giancola, C. The triazatruxene derivative azatrux binds to the parallel form of the human telomeric G-quadruplex under molecular crowding conditions: biophysical and molecular modeling studies. *Biochimie* **2011**, *93*, 1318–1327.
- (18) Pagano, B.; Cosconati, S.; Gabelica, V.; Petraccone, L.; De Tito, S.; Marinelli, L.; La Pietra, V.; Di Leva, F. S.; Lauri, I.; Trotta, R.; Novellino, E.; Giancola, C.; Randazzo, A. State-of-the-art methodologies for the discovery and characterization of DNA G-quadruplex binders. *Curr. Pharm. Des.* **2012**, *18*, 1880–1899.
- (19) Horton, D. A.; Bourne, G. T.; Smythe, M. L. The combinatorial synthesis of bicyclic privileged structures or privileged substructures. *Chem. Rev.* **2003**, *103*, 893–930.
- (20) Velazquez Campoy, A.; Freire, E. ITC in the post-genomic era...? Priceless. *Biophys. Chem.* **2005**, *115*, 115–124.
- (21) (a) Pagano, B.; Mattia, C. A.; Virno, A.; Randazzo, A.; Mayol, L.; Giancola, C. Thermodynamic analysis of quadruplex DNA-drug interaction. *Nucleosides, Nucleotides Nucleic Acids* **2007**, *26*, 761–765. (b) Pagano, B.; Mattia, C. A.; Giancola, C. Applications of isothermal titration calorimetry in biophysical studies of G-quadruplexes. *Int. J. Mol. Sci.* **2009**, *10*, 2935–2957.
- (22) Klevit, R. E.; Wemmer, D. E.; Reid, B. R. <sup>1</sup>H NMR studies on the interaction between distamycin A and a symmetrical DNA dodecamer. *Biochemistry* **1986**, *25*, 3296–3303.
- (23) van Telesens, B.; de Lange, T. Control of telomere length by the human telomeric protein TRF1. *Nature* **1997**, *385*, 740–743.
- (24) Takai, H.; Smogorzewska, A.; de Lange, T. DNA damage foci at dysfunctional telomeres. *Curr. Biol.* **2003**, *13*, 1549–1556.
- (25) (a) Yu, H.; Wang, X.; Fu, M.; Ren, J.; Qu, X. Chiral metallo-supramolecular complexes selectively recognize human telomeric G-quadruplex DNA. *Nucleic Acids Res.* **2008**, *36*, 5695–5703. (b) Yu, H.; Zhao, C.; Chen, Y.; Fu, M.; Ren, J.; Qu, X. DNA loop sequence as the determinant for chiral supramolecular compound G-quadruplex selectivity. *J. Med. Chem.* **2010**, *53*, 492–498.
- (26) For example, see the following: (a) D'Onofrio, J.; Petraccone, L.; Martino, L.; Di Fabio, G.; Iadonisi, A.; Balzarini, J.; Giancola, C.; Montesarchio, D. Synthesis, biophysical characterization, and anti-HIV activity of glyco-conjugated G-quadruplex-forming oligonucleotides.

*Bioconjugate Chem.* **2008**, *19*, 607–616. (b) Di Fabio, G.; D'Onofrio, J.; Chiapparelli, M.; Hoorelbeke, B.; Montesarchio, D.; Balzarini, J.; De Napoli, L. Discovery of novel anti-HIV active G-quadruplex-forming oligonucleotides. *Chem. Commun.* **2011**, *47*, 2363–2365.

(27) Hwang, T. L.; Shaka, A. J. J. Water suppression that works. Excitation sculpting using arbitrary waveforms and pulsed field gradients. *J. Magn. Reson.* **1995**, *A112*, 275–279.

(28) Dalvit, C. Efficient multiple-solvent suppression for the study of the interactions of organic solvents with biomolecules. *J. Biomol. NMR* **1998**, *11*, 437–444.

(29) Cantor, C. R.; Warshaw, M. M.; Shapiro, H. Oligonucleotide interactions. 3. Circular dichroism studies of the conformation of deoxyoligonucleotides. *Biopolymers* **1970**, *9*, 1059–1077.

(30) Biroccio, A.; Amodei, S.; Benassi, B.; Scarsella, M.; Cianciulli, A.; Mottolise, M.; Del Bufalo, D.; Leonetti, C.; Zupi, G. Reconstitution of hTERT restores tumorigenicity in melanoma-derived c-Myc low-expressing clones. *Oncogene* **2002**, *21*, 3011–3019.

(31) Biroccio, A.; Benassi, B.; Filomeni, G.; Amodei, S.; Marchini, S.; Chiorino, G.; Rotilio, G.; Zupi, G.; Ciriolo, M. R. Glutathione influences c-Myc-induced apoptosis in M14 human melanoma cells. *J. Biol. Chem.* **2002**, *277*, 43763–43770.

(32) Dimri, G. P.; Lee, X.; Basile, G.; Acosta, M.; Scott, G.; Roskelley, C.; Medrano, E. E.; Linskens, M.; Rubelj, I.; Pereira-Smith, O.; Peacocke, M.; Campisi, J. A biomarker that identifies senescent human cells in culture and in aging skin in vivo. *Proc. Natl. Acad. Sci. U.S.A.* **1995**, *92*, 9363–9367.